

Highly Selective and Sensitive Trimethylamine Gas Sensor Based on Cobalt Imidazolate Framework Material

Er-Xia Chen,^{†,‡} Hong-Ru Fu,[†] Rui Lin,[†] Yan-Xi Tan,[†] and Jian Zhang^{*,†}

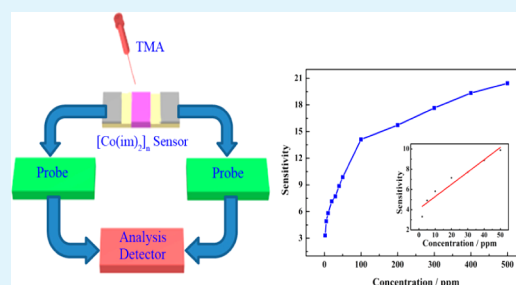
[†]State Key Laboratory of Structural Chemistry, Fujian Institute of Research on the Structure of Matter, Chinese Academy of Sciences, Fuzhou, Fujian 350002, People's Republic of China

[‡]College of Materials Science and Engineering, Fuzhou University, Fuzhou, Fujian 350108, People's Republic of China

S Supporting Information

ABSTRACT: A cobalt imidazolate (im) framework material $[\text{Co}(\text{im})_2]_n$ was employed to use as a trimethylamine (TMA) gas sensor and the $[\text{Co}(\text{im})_2]_n$ sensor can be easily fabricated by using Ag–Pd interdigitated electrodes. Gas sensing measurement indicated that the $[\text{Co}(\text{im})_2]_n$ sensor shows excellent selectivity, high gas response and a low detection limit level of 2 ppm to TMA at 75 °C. The good selectivity and high response to TMA of the sensor based on $[\text{Co}(\text{im})_2]_n$ may be attributed to the weak interaction between the TMA molecules and the $[\text{Co}(\text{im})_2]_n$ framework. That may provide an ideal candidate for detecting freshness of fish and seafood.

KEYWORDS: cobalt imidazolate framework, gas sensor, selectivity, trimethylamine



INTRODUCTION

Trimethylamine (TMA) is known to be a colorless and toxic gas, which could cause headache and stimulate eyes and the respiratory system. TMA has also drawn significant attention in recent years because it could be one of effective indicators for assessment of fish and seafood freshness.¹ TMA is usually generated from microbial degradation of trimethylamine N-oxide during the deteriorating of fish and seafood.^{2–4} The concentration of TMA will rise with the degree of decaying fish and seafood. Therefore, researchers have defined the freshness degree based on the concentration of TMA released from fish and seafood (fresh, <10 ppm; preliminary rot, 10–50 ppm; corruption, >60 ppm).^{5,6}

It has been known that lots of gas sensors based on metal oxide semiconductors display response to TMA.^{7–19} For examples, WO_3 hollow spheres sensor exhibited high response (56.9) to 5 ppm TMA at 450 °C.¹⁰ Zhang and his co-workers reported the sensor based on $\alpha\text{-Fe}_2\text{O}_3/\text{TiO}_2$ and the response to 50 ppm TMA reached 13.9 at 250 °C.¹¹ The Ru-doped SnO_2 sensor showed good response (99.1) to 5 ppm TMA at 350 °C.¹² The sensor based on MoO_3 microrods revealed excellent gas performance to TMA and the response achieved 1.5 to 0.01 ppm TMA at 300 °C.¹³ The response (17.9) of the sensor based on Cr_2O_3 -decorated ZnO to 5 ppm TMA was remarkable at 400 °C.⁶ The response of flowerlike In_2O_3 attained 5.9 to 5 ppm TMA at 340 °C.¹⁴ However, it is still difficult for metal oxide semiconductors to obtain outstanding gas-sensing property at low operating temperatures.

Due to their prominent chemical and thermal stability, metal imidazolate framework materials have great potential applications in chemical sensing, magnetic property, catalysis, gas capture and separation.^{20–28} In spite of the development in gas

capture and separation, the reports on the applications of these metal imidazolate frameworks as gas sensors are infrequent.^{29–32} Compared with the metal oxide semiconductors, most of metal imidazolate framework materials possess high surface areas.^{33,34} Moreover, some sensors based on these materials could work at low operating temperatures.^{29–32}

Here, we report a cobalt-imidazole framework ($[\text{Co}(\text{im})_2]_n$, im = imidazole) as a gas sensor for TMA at a low operating temperature (75 °C).³⁵ Excellent selectivity and gas response to TMA are successfully achieved. The $[\text{Co}(\text{im})_2]_n$ sensor could measure TMA as low as 2 ppm, and the response is 2.5 at 75 °C. The results indicate that the $[\text{Co}(\text{im})_2]_n$ sensor may be a promising detector to assess the degree of fish and seafood freshness.

EXPERIMENTAL SECTION

Chemicals. $\text{Co}(\text{CH}_3\text{COO})_2 \cdot 4\text{H}_2\text{O}$ was purchased from Aladdin company. Ethyleneurea hemihydrates and imidazole were purchased from Alfa Aesar, and ethanol was purchased from Sinopharm. All chemical reagents were used without further purification.

Synthesis of $[\text{Co}(\text{im})_2]_n$. $\text{Co}(\text{CH}_3\text{COO})_2 \cdot 4\text{H}_2\text{O}$ (0.498 g, 2 mmol), imidazole (0.544 g, 4 mmol), ethyleneurea hemihydrates (2 g) and ethanol (1 mL) were mixed in a 23 mL Teflon-lined stainless steel container and heated to 140 °C for 6 days, and then cooled to room temperature. Purple $[\text{Co}(\text{im})_2]_n$ crystals were obtained after washing thrice with ethanol. The crystal data for $[\text{Co}(\text{im})_2]_n$: $a = b = 23.437(6)$ Å, $c = 12.508(3)$ Å, $V = 6870$ Å³, tetragonal, space group: $I4_1cd$.

Received: October 16, 2014

Accepted: November 24, 2014

Published: November 24, 2014

Characterization. UV–vis diffuse reflectance spectra were carried out on the Varian Cary 500 UV–vis spectrophotometer. A Netzsch STA 449C thermal analyzer were employed for thermal analysis at a temperature range of 30 to 800 °C under air atmosphere and nitrogen atmosphere, respectively, with a heating rate of 10 °C·min⁻¹. A Rigaku Dmax 2500 X-ray diffractometer with Cu K α radiation ($\lambda = 1.54056$ Å) was used to record the powder X-ray diffraction (PXRD) of the synthesized and after heating sample in the air, investigating the thermal stability of [Co(im)₂]_n in the air atmosphere. The X-ray photoelectron spectroscopy (XPS) measurements were performed on a Thermo Scientific ESCALAB 250 with a monochromatic Al K α source. The gas adsorption measurements were carried out on a Micromeritics ASAP 2020 surface area and pore size analyzer. Scanning electron microscopy (SEM) images were obtained by a JSM-6700F.

Preparation of [Co(im)₂]_n Sensor. The paste was prepared from ground [Co(im)₂]_n with an appropriate amount of ethanol and then the paste was coated on the interdigital electrodes of the sensor substrates by a tiny brush. With five pairs of Ag–Pd interdigitated electrodes (Figure 1a, both the distance and width were 200 μ m), the

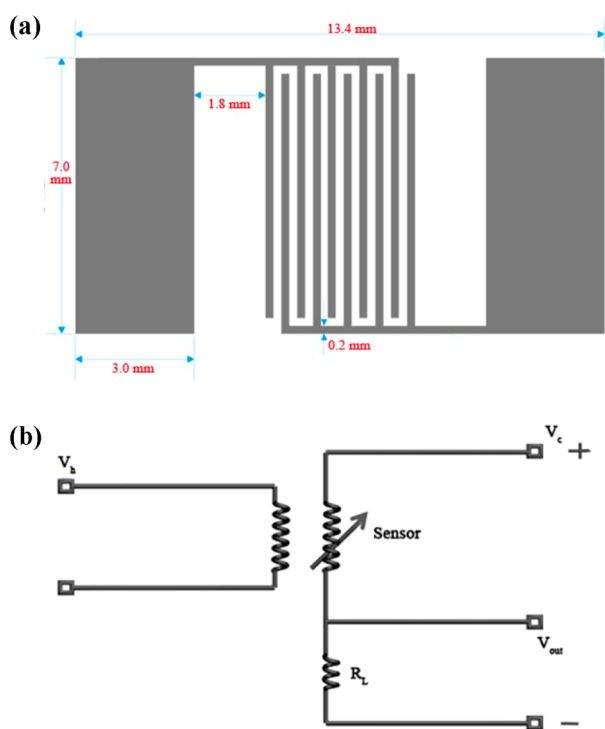


Figure 1. (a) Structure of Ag–Pd interdigitated electrode; (b) Image of operating principle.

sensor substrates (13.4 \times 7 mm, 0.5 mm in the thickness) were bought from Beijing Elite Tech Co., Ltd. The prepared sensors are presented in Figure S1 (Supporting Information). The coated sensors eliminated ethanol at 80 °C in the furnace and then were calcined at 200 °C for 1.5 h.

Gas-Sensing Measurement. Gas sensing experiments were carried out on the CGS-1TP intelligent gas sensing analysis system (Beijing Elite Tech Co., Ltd., China). In process testing, corresponding amounts of methanol, formaldehyde, acetone, ammonia, trimethylamine, triethylamine were injected into evaporator in the test box by a microsyringe and methane was directly injected into the test box. The air served as the diluting gas and the reference gas.

Principle of Gas-Sensing Measurement. Figure 1b displays the graphic testing principle. The heating voltage (V_h) was used to heat the sensor. The load resistance and the sensor were connected in series and a circuit voltage (V_c) was applied on them. The output

voltage (V_{out}) was exerted to the load resistance which could change with the variety and concentration of measured gas.

Here, the response value of the [Co(im)₂]_n sensor is depicted as R_g/R_a , R_g and R_a meaning the resistance in the target gas and air, respectively. Response time is defined as the time needed for the sensor to obtain 90% of the total resistance change in the response and in the case of recovery described as recovery time.

RESULTS AND DISCUSSION

Polymer [Co(im)₂]_n possesses a 3D structure with zni topology (Figure 2). The band gap of [Co(im)₂]_n was studied by the

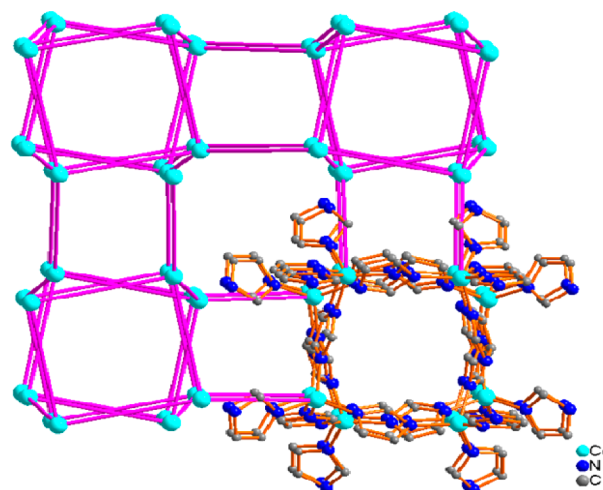


Figure 2. zni-Type structure of [Co(im)₂]_n.

UV–vis diffuse reflection method at room temperature (Figure 3). The absorption edge energy ($E_g = 1.80$) was estimated

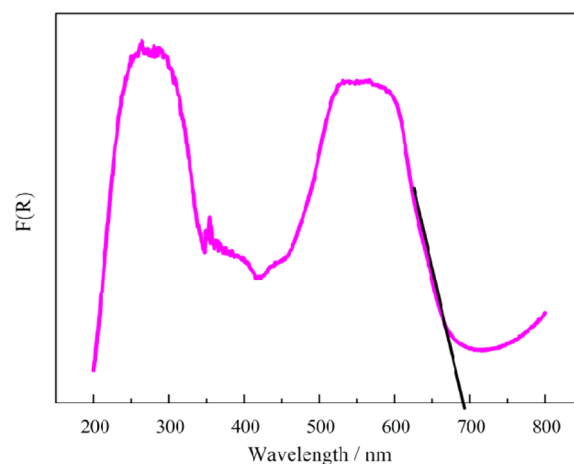


Figure 3. UV–vis diffuse reflectance spectrum of [Co(im)₂]_n.

according to the equation $ah\nu^2 = K(h\nu - E_g)^{1/2}$ (where K is the constant, $h\nu$ is discrete photoenergy and α is the absorption coefficient) when α is equal to zero. Thermogravimetric analyses (TGA, Figure 4) in the air and powder X-ray diffraction (PXRD) experiments (Figure 5) at different temperatures in the air were carried out to investigate the chemical and thermal stability of [Co(im)₂]_n. The PXRD patterns below 250 °C in the air match with the simulated pattern from single-crystal XRD structure, which demonstrate that the framework of [Co(im)₂]_n is stable below 250 °C in the air. The PXRD patterns after TMA detection are also

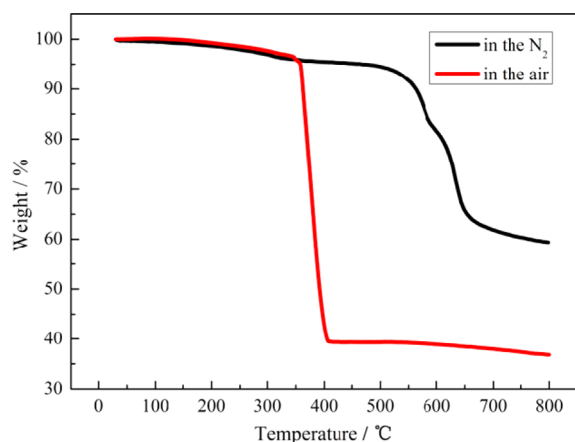


Figure 4. TGA curves of $[\text{Co}(\text{im})_2]_n$ in the N_2 and air atmosphere.

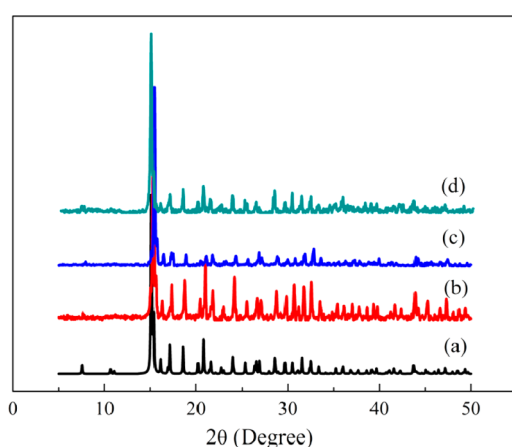


Figure 5. PXRD patterns of $[\text{Co}(\text{im})_2]_n$: (a) simulated $[\text{Co}(\text{im})_2]_n$; (b) as-synthesized $[\text{Co}(\text{im})_2]_n$; (c) $[\text{Co}(\text{im})_2]_n$ after heating at 250°C in the air atmosphere for 10 h; (d) $[\text{Co}(\text{im})_2]_n$ after TMA detection.

coincident with the patterns simulated, which shows that the $[\text{Co}(\text{im})_2]_n$ is chemical stability. The sorption isotherms of CO_2 for $[\text{Co}(\text{im})_2]_n$ were obtained up to 1 bar at 273 K (Figure S2, Supporting Information). The CO_2 uptake value is $36\text{ cm}^3/\text{g}$ at 273 K and 1 bar, revealing the porosity presented in the structure of $[\text{Co}(\text{im})_2]_n$. The XPS spectra measurements were carried out to confirm the valence state of Co in both as-synthesized $[\text{Co}(\text{im})_2]_n$ and the $[\text{Co}(\text{im})_2]_n$ after TMA detection (Figure S3, Supporting Information). The results indicate that the oxidation states of the Co element in the $[\text{Co}(\text{im})_2]_n$ at the different conditions are the same, because the characteristic peaks do not change. The as-synthesized crystals of $[\text{Co}(\text{im})_2]_n$ were ground to powder and then coated on the Ag–Pd interdigitated electrodes for gas sensing measurements.

The responses to 100 ppm diverse gases (methanol, formaldehyde, acetone, ammonia, trimethylamine, triethylamine and methane) were measured as the function of the sensor temperature (Figure 6). Obviously, the response increases at first and reaches maximum (14.1) to TMA at 75°C and then decreases with further improving operating temperature. Hence, the optimum operating temperature of the $[\text{Co}(\text{im})_2]_n$ sensor to TMA was defined as about 75°C . In comparison, at the optimum operating temperature, the responses to formaldehyde (5.7) and triethylamine (8.9) are low. Moreover, it is worth noting that the responses to methanol (1.9), acetone (2.6), ammonia (1.4) and methane

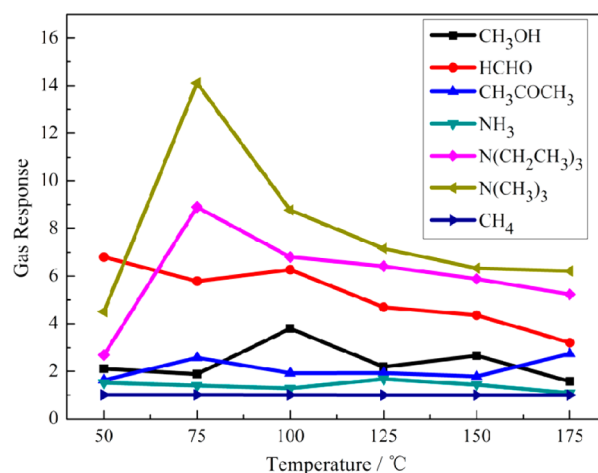


Figure 6. Sensitivity of $[\text{Co}(\text{im})_2]_n$ sensor to 100 ppm various gases in the temperature range $50\text{--}175^\circ\text{C}$.

(1.1) are infirm and could be ignored, compared to TMA. It reveals that the $[\text{Co}(\text{im})_2]_n$ sensor possesses excellent selectivity to TMA at about 75°C .

The transients to 2–500 ppm TMA of the $[\text{Co}(\text{im})_2]_n$ sensor at 75°C were also investigated (real-time gas sensing transients to 2–500 ppm TMA are shown in Figure S4, Supporting Information). As shown in Figure 7, the response values fleetly

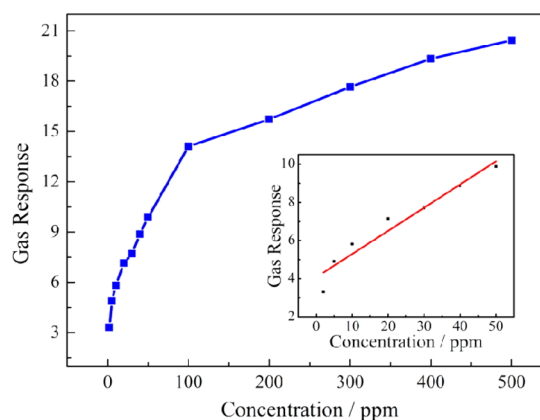


Figure 7. Response of the $[\text{Co}(\text{im})_2]_n$ sensor to different concentration TMA at 75°C . The inset presents a linear dependence of response on TMA concentration between 2 and 50 ppm.

raise with increasing of TMA concentration from 2 to 500 ppm. The response reaches 20.4 when the $[\text{Co}(\text{im})_2]_n$ sensor exposes 500 ppm TMA. It is worthwhile to note that there is good linearity between TMA concentration and sensitivity in the low concentration scope (2–50 ppm) (Figure 7 inset). It is well-known that the concentration of TMA released by fish and seafood gradually increases with the decrease in freshness. Therefore, the $[\text{Co}(\text{im})_2]_n$ sensor may serve as not only a sensitive material for TMA detection but also a candidate to measure the freshness of fish.

The response–recovery feature is an essential parameter for the gas sensors. As shown in Figure 8, the response time and recovery time are relative slow, which need improvements in the future. This may be ascribed to the reason that the operating temperature is low (only 75°C). Because it is a process associated with operating temperature to form and destroy the weak interaction between sensing material and

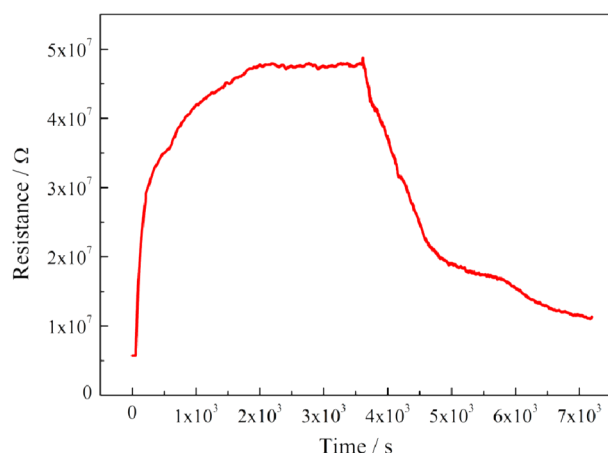


Figure 8. Real-time gas-sensing transients of the sensor based on $[\text{Co}(\text{im})_2]_2$ to 100 ppm TMA at 75 °C.

detected gas. And this can be demonstrated by improving the operating temperature (Figure S5, Supporting Information).

The stability is also a crucial property for the gas sensor and the sensing measurements to 100 ppm TMA were operated every 8 days to study the stability of the $[\text{Co}(\text{im})_2]_n$ sensor. The gas response (in 24 days) shows a little decrease from 15.4 to 14.0 (Figure 9) in the air, indicating the excellent stability of the $[\text{Co}(\text{im})_2]_n$ sensor.

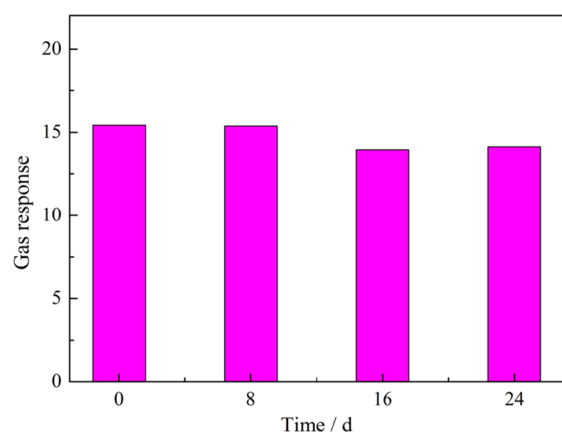


Figure 9. Responses of $[\text{Co}(\text{im})_2]_n$ sensor to 100 ppm TMA in different days.

Moreover, the relationship of environmental humidity and gas response to 100 ppm TMA is also investigated (Figure 10). It is obvious that there is a less important impact when ambient humidity is inferior to 70% so that it can be ignored. However, above 70%, environmental humidity makes a great impact on the gas-sensing properties of the $[\text{Co}(\text{im})_2]_n$ sensor. The sensitivity to 100 ppm TMA reduces to 10.3 when the relative humidity comes to 84%.

The good selectivity and high response to TMA of the sensor based on $[\text{Co}(\text{im})_2]_n$ may be explained as follows. Compared with the O atoms in the methanol, formaldehyde or acetone, N atoms in $(\text{CH}_3)_3\text{N}$ possess higher cloud density because of the electronic donation of $-\text{CH}_3$ groups. This may be conducive to cause weak interactions between the $(\text{CH}_3)_3\text{N}$ molecules and the $[\text{Co}(\text{im})_2]_n$ framework. Such weak interactions have contributed to absorb TMA on $[\text{Co}(\text{im})_2]_n$, and then cause a greater change in resistance. By comparison, there may be a

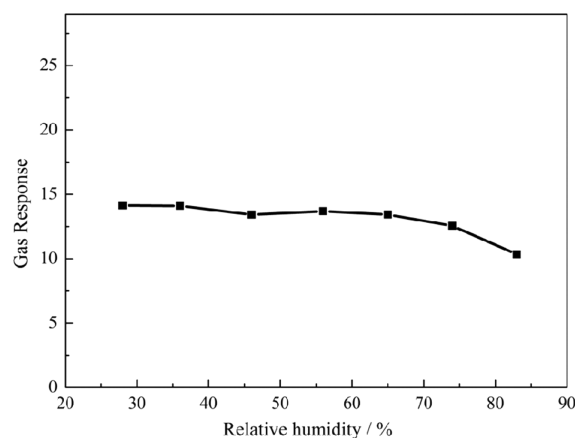


Figure 10. $[\text{Co}(\text{im})_2]_n$ sensor response to 100 ppm TMA at various humidity conditions.

slightly larger steric hindrance in $(\text{CH}_3\text{CH}_2)_3\text{N}$ than in $(\text{CH}_3)_3\text{N}$. Therefore, the response to $(\text{CH}_3\text{CH}_2)_3\text{N}$ is a little lower than that to $(\text{CH}_3)_3\text{N}$. The interactions between ammonia, methane and $[\text{Co}(\text{im})_2]_n$ can be ignored, and it is difficult to absorb ammonia and methane on $[\text{Co}(\text{im})_2]_n$. Thus, the response values to ammonia and methane are low.

CONCLUSION

In summary, the $[\text{Co}(\text{im})_2]_n$ sensor with prominent selective, high response and a detection limit level of 2 ppm to TMA at low operating temperature (75 °C), may be a desirable candidate for examining the freshness of fish and seafood in actual practice. The response to TMA at low operating temperatures (about 75 °C) may be ascribed to the weak interactions between $[\text{Co}(\text{im})_2]_n$ and TMA. The results demonstrated that the inorganic–organic hybrid materials with low band gaps can be good gas sensors.

ASSOCIATED CONTENT

Supporting Information

Pictures of $[\text{Co}(\text{im})_2]_n$ sensor, CO_2 sorption isotherms, the XPS spectra, the real-time gas-sensing transients of the sensor based on $[\text{Co}(\text{im})_2]_n$ to different TMA concentrations at 75 °C and the SEM image of $[\text{Co}(\text{im})_2]_n$. This material is available free of charge via the Internet at <http://pubs.acs.org>.

AUTHOR INFORMATION

Corresponding Author

*J. Zhang. E-mail: zhj@fjirsm.ac.cn.

Notes

The authors declare no competing financial interest.

ACKNOWLEDGMENTS

This work is supported by 973 program (2012CB821705 and 2011CB932504), NSFC (91222105, 21221001), and CAS (XDA07070200).

REFERENCES

- (1) Yang, R.; Huang, X.; Wang, Z.-Y.; Zhou, Y.-Z.; Liu, L.-T. A Chemisorption-based Microcantilever Chemical Sensor for the Detection of Trimethylamine. *Sens. Actuators, B* **2010**, *145*, 474–479.
- (2) Qi, Q.; Zou, Y.-C.; Fan, M.-H.; Liu, Y.-P.; Gao, S.; Wang, P.-P.; He, Y.; Wang, D.-J.; Li, G.-D. Trimethylamine Sensors with Enhanced

Anti-humidity Ability Fabricated from $\text{La}_{0.7}\text{Sr}_{0.3}\text{FeO}_3$ Coated In_2O_3 - SnO_2 Composite Nanofibers. *Sens. Actuators, B* **2014**, *203*, 111–117.

(3) Cho, Y. H.; Ko, Y. N.; Kang, Y. C.; Kim, D.; Lee, J.-H. Ultrasensitive and Ultrasensitive Detection of Trimethylamine Using MoO_3 Nanoplates Prepared by Ultrasonic Spray Pyrolysis. *Sens. Actuators, B* **2014**, *195*, 189–196.

(4) Du, J.-P.; Wang, H.-Y.; Zhao, R.-H.; Xie, Y.-J.; Yao, H.-L. Surfactant-Assisted Synthesis of the Pencil-like Zinc Oxide and Its Sensing Properties. *Mater. Lett.* **2013**, *107*, 259–261.

(5) Mitsubayashi, K.; Kubotera, Yano, K.; Hashimoto, Y.; Takuo, K.; Nakakura, S.; Nishi, Y.; Endo, H. Trimethylamine Biosensor with Flavin-Containing Monooxygenase Type 3 (FMO₃) for Fish-Freshness Analysis. *Sens. Actuators B* **2004**, *103*, 463–467.

(6) Woo, H.-S.; Na, C. W.; Kim, D.; Lee, J.-H. Highly Sensitive and Selective Trimethylamine Sensor Using One-Dimensional $\text{ZnO}-\text{Cr}_2\text{O}_3$ Hetero-nanostructures. *Nanotechnology* **2012**, *23*, 245501.

(7) Zhang, W.-H.; Zhang, W.-D. Fabrication of SnO_2 - ZnO Nanocomposite Sensor for Selective Sensing of Trimethylamine and the Freshness of Fishes. *Sens. Actuators, B* **2008**, *134*, 403–408.

(8) Chu, X.-F.; Liang, S.-M.; Chen, T.-Y.; Zhang, Q.-F. Trimethylamine Sensing Properties of $\text{CdO}-\text{Fe}_2\text{O}_3$ Nano-materials Prepared Using Co-precipitation Method in the Presence of PEG400. *Mater. Chem. Phys.* **2010**, *123*, 396–400.

(9) Jung, J.-Y.; Lee, C.-S. Characteristics of the $\text{TiO}_2/\text{SnO}_2$ Thick Film Semiconductor Gas Sensor to Determine Fish Freshness. *J. Ind. Eng. Chem.* **2011**, *17*, 237–242.

(10) Cho, Y. H.; Kang, Y. C.; Lee, J.-H. Highly Selective and Sensitive Detection of Trimethylamine Using WO_3 Hollow Spheres Prepared by Ultrasonic Spray Pyrolysis. *Sens. Actuators, B* **2013**, *177*, 917–977.

(11) Lou, Z.; Li, F.; Deng, J.-N.; Wang, L.-L.; Zhang, T. Branch-like Hierarchical Heterostructure ($\alpha\text{-Fe}_2\text{O}_3/\text{TiO}_2$): A Novel Sensing Material for Trimethylamine Gas Sensor. *ACS Appl. Mater. Interfaces* **2013**, *5*, 12310–12316.

(12) Kim, K.-M.; Choi, K.; Jeong, H.-M.; Kim, H.-J.; Kim, H.-R.; Lee, J.-H. Highly Sensitive and Selective Trimethylamine Sensors Using Ru-Doped SnO_2 Hollow Spheres. *Sens. Actuators, B* **2012**, *166*–*167*, 733–738.

(13) Chu, X.-F.; Liang, S.-M.; Sun, W.-Q.; Zhang, W.-B.; Chen, T.-Y.; Zhang, Q.-F. Trimethylamine Sensing Properties of Sensors Based on MoO_3 Microrods. *Sens. Actuators, B* **2010**, *148*, 399–403.

(14) Lu, X.-F.; Yu, Q.-Q.; Wang, K.; Shi, L.-C.; Liu, X.; Qiu, A.-G.; Wang, L.; Cui, D.-L. Synthesis, Characterization and Gas Sensing Properties of Flowerlike In_2O_3 Composed of Microrods. *Cryst. Res. Technol.* **2010**, *45*, 557–561.

(15) Wang, L.-L.; Fei, T.; Lou, Z.; Zhang, T. Three-Dimensional Hierarchical Flowerlike $\alpha\text{-Fe}_2\text{O}_3$ Nanostructures: Synthesis and Ethanol-Sensing Properties. *ACS Appl. Mater. Interfaces* **2011**, *3*, 4689–4694.

(16) Wu, M.-Z.; Zhang, X.-F.; Gao, S.; Cheng, X.-L.; Rong, Z.-M.; Xu, Y.-M.; Zhao, H.; Huo, L.-H. Construction of Monodisperse Vanadium Pentoxide Hollow Spheres via a Facile Route and Triethylamine Sensing Property. *CrystEngComm* **2013**, *15*, 10123–10131.

(17) Wang, L.-L.; Deng, J.-N.; Lou, Z.; Zhang, T. Cross-Linked *p*-Type Co_3O_4 Octahedral Nanoparticles in 1D *n*-Type TiO_2 Nanofibers for High-Performance Sensing Devices. *J. Mater. Chem. A* **2014**, *2*, 10022–10028.

(18) Wang, X.-F.; Ding, B.; Yu, J.-Y.; Si, Y.; Yang, S.-B.; Sun, G. Electro-Netting: Fabrication of Two-Dimensional Nano-nets for Highly Sensitive Trimethylamine Sensing. *Nanoscale* **2011**, *3*, 911–915.

(19) Wang, L.-L.; Dou, H.-M.; Lou, Z.; Zhang, T. Encapsulated Nanoreactors ($\text{Au}@\text{SnO}_2$): A New Sensing Material for Chemical Sensors. *Nanoscale* **2013**, *5*, 2686–2691.

(20) Park, K. S.; Ni, Z.; Côté, A. P.; Choi, J. Y.; Huang, R. D.; Uribe-Romo, F. J.; Chae, H. K.; O'Keeffe, M.; Yaghi, O. M. Exceptional Chemical and Thermal Stability of Zeolitic Imidazolate Frameworks. *Proc. Natl. Acad. Sci. U. S. A.* **2006**, *103*, 10186–10191.

(21) Biswal, B. P.; Panda, T.; Banerjee, R. Solution Mediated Phase Transformation (RHO to SOD) in Porous Co-imidazolate Based Zeolitic Frameworks with High Water Stability. *Chem. Commun.* **2012**, *48*, 11868–11870.

(22) Liu, B. Metal–Organic Framework-based Devices: Separation and Sensors. *J. Mater. Chem.* **2012**, *22*, 10094–10101.

(23) Tian, Y.-Q.; Chen, Z.-X.; Weng, L.-H.; Guo, H.-B.; Gao, S.; Zhao, D.-Y. Two Polymorphs of Cobalt(II) Imidazolate Polymers Synthesized Solvothermally by Using One Organic Template *N,N*-Dimethylacetamide. *Inorg. Chem.* **2004**, *43*, 4631–4635.

(24) Banerjee, R.; Phan, A.; Wang, B.; Knobler, C.; Furukawa, H.; O'Keeffe, M.; Yaghi, O. M. High-Throughput Synthesis of Zeolitic Imidazolate Frameworks and Application to CO_2 Capture. *Science* **2008**, *319*, 939–943.

(25) Liu, B.; Smit, B. Molecular Simulation Studies of Separation of CO_2/N_2 , CO_2/CH_4 and CH_4/N_2 by ZIFs. *J. Phys. Chem. C* **2010**, *114*, 8515–8522.

(26) Dey, C.; Banerjee, R. Controlled Synthesis of a Catalytically Active Hybrid Metal-oxide Incorporated Zeolitic Imidazolate Framework (MOZIF). *Chem. Commun.* **2013**, *49*, 6617–6619.

(27) Wang, F.; Liu, Z.-S.; Yang, H.; Tan, Y.-X.; Zhang, J. Hybrid Zeolitic Imidazolate Frameworks with Catalytically Active TO_4 Building Blocks. *Angew. Chem., Int. Ed.* **2011**, *50*, 450–453.

(28) Yang, H.; He, X.-W.; Wang, F.; Kang, Y.; Zhang, J. Doping Copper into ZIF-67 for Enhancing Gas Uptake Capacity and Visible-light-driven Photocatalytic Degradation of Organic Dye. *J. Mater. Chem.* **2012**, *22*, 21849–21851.

(29) Cheng, X.; Zhang, Y.; Wang, G.-P.; Zhang, Y.-P.; Lu, B.-W.; Ruan, S.-P.; Liu, C.-X. Humidity Sensing Properties of Metal-Organic Framework Materials of ZIF-8 (12). *China Scientific and Technical Papers* **2013**, *8*, 355–358.

(30) Chen, E.-X.; Yang, H.; Zhang, J. Zeolitic Imidazolate Framework as Formaldehyde Gas Sensor. *Inorg. Chem.* **2014**, *53*, 5411–5413.

(31) Hwang, Y.; Sohn, H.; Phan, A.; Yaghi, O. M.; Candler, R. N. Dielectrophoresis-Assembled Zeolitic Imidazolate Framework Nanoparticle-Coupled Resonators for Highly Sensitive and Selective Gas Detection. *Nano Lett.* **2013**, *13*, 5271–5276.

(32) Hwang, Y.; Phan, A.; Galatsis, K.; Yaghi, O. M.; Candler, R. N. Zeolitic Imidazolate Framework-Coupled Resonators for Enhanced Gas Detection. *J. Micromech. Microeng.* **2013**, *23*, 1–5.

(33) Tian, Y.-Q.; Yao, S.-Y.; Gu, D.; Cui, K.-H.; Guo, D.-W.; Zhang, G.; Chen, Z.-X.; Zhao, D.-Y. Cadmium Imidazolate Frameworks with Polymorphism, High Thermal Stability, and a Large Surface Area. *Chem.—Eur. J.* **2010**, *16*, 1137–1141.

(34) Phan, A.; Doonan, C. J.; Uribe-romo, F. J.; Knobler, C. B.; O'Keeffe, M.; Yaghi, O. M. Synthesis, Structure, and Carbon Dioxide Capture Properties of Zeolitic Imidazolate Frameworks. *Acc. Chem. Res.* **2010**, *43*, 58–67.

(35) Tian, Y.-Q.; Cai, C.-X.; Ren, X.-M.; Duan, C.-Y.; Xu, Y.; Gao, S.; You, X.-Z. The Silica-Like Extended Polymorphism of Cobalt(II) Imidazolate Three-Dimensional Frameworks: X-ray Single-Crystal Structures and Magnetic Properties. *Chem.—Eur. J.* **2003**, *9*, 5673–5685.